Research on Two-channel Interleaved Two-stage Paralleled Buck DC-DC Converter for Plasma Cutting Power Supply

XI-JUN YANG[1], CHEN YAO[1], NING-YUN ZHANG[1], HAO QU[1], HOU-JUN TANG[1], FREDE BLAABJERG[2]
[1] Key Lab. of Power Transmission and Conversion Control (Ministry of Education), [2]Dept. of Energy Technology
[1]Shanghai Jiao Tong University, [2]Faculty of Engineering and Science, Aalborg University
[1]Shanghai China 200240, [2]Aalborg Denmark 9220
[1]P.R. CHINA, [2]DENMARK
youngxijun@163.com

Abstract: - Buck DC-DC converter is an important and typical power electronic converter with relatively simple topology and rich study contents. Nowadays, it has been widely used as SMPS and high power DC power supplies. As for high power plasma cutting machine, multi-channel interleaved and multi-stage paralleled buck DC-DC converter is the first choice. When designed as a constant DC current supply, it is characteristic of high current precision, good stability and reliability, and it can be designed with current limitation, power equilibrium, constant switching frequency, zero output current steady-state error and phase shift driving. In the paper, a two-channel interleaved, two-stage paralleled buck DC-DC converter is analyzed and designed by using sliding mode control (SMC) and simulated by means of MATLAB/SIMULINK. The basic principle of sliding mode control is also reviewed. Then the experimental setup of plasma cutting machine (PCM) DC current supply is implemented on the basis of the theoretical analysis, which outputs the rated current of 260A and the rated DC voltage of 150V, and the switching frequency is selected as 10kHz. The gained results prove the designed sliding mode control.

Key-Words: - Plasma cutting power supply, buck DC-DC converter, Two-channel interleaved, Two-stage paralleled, Sliding mode control, Current limitation, Constant switching frequency, Output voltage steady-state error, Phase shift driving

1 Introduction

Cutter and welder is well known as the tailor of steel industry, widely used as key technologies in the fields of bridge, construction, machinery, shipping, railway, metallurgy, petrochemical, water power generation, home appliance, container, boiler pressure vessel, power generation equipment industry, etc. Cutting is the first procedure of metal welding, ready for subsequent processing and welding. The metal cutting includes hot cutting and cold cutting, and the former is the most widely used, including flame cutting machine, plasma cutting machine (PCM) and laser cutting machine. Plasma cutting machine has a long range of applications, due to high cutting speed, high cutting thickness and better cutting quality, which is near laser cutting. The generation of plasma arc column needs plasma DC current power supply. Plasma power supply has gone through three technological innovations, they are, silicon rectifier DC power supply, thyristor rectifier DC power supply, and IGBT DC-DC power supply[1-5]. The last type includes the isolation DC-DC converter (below 20kW) and the non-isolation buck DC-DC converter (above 20kW). Multi-channel interleaved, multi-stage paralleled buck DC-DC converter is the first candidate for high power PCM, because such converter can support high DC current (above 130A per sub-module) and has simple power stage and control stage, simple design, low overall cost.

As a switching mode power supply (SMPS), buck DC-DC converter has a lot of control methods. Due to nonlinear and time-varying property, nonlinear control approaches should be considered in the first place, though it is a challenging task to get high-performance control. The controller should bring about satisfactory static and dynamic performances and make the system rugged and stable in the presence of input voltage disturbance, load power change and system parameter variation. Sliding mode control (SMC) is one of the control approaches based on variable structure systems (VSS), defined as a system where the circuit topology is intentionally changed according to a certain control rule, in order to improve the system

behavior in terms of response speed, global stability, and robustness.

VSS involves a certain number of independent sub-topologies, which are determined by the status of nonlinear elements (switches). The global dynamics of VSS is quite different from each sub-topology. There are many references provide systematical analyses of VSS and sliding mode control [6,7]. Sliding mode control was employed to the field of DC-DC converter earlier[8], and a great deal of work was done to improve sliding mode control effectiveness in terms of current limitation[9-12], power equilibrium[13,14], reduced or constant switching frequency[15-16], zero output current steady-state error and phase shift driving[14,17,18]. In the paper, mainly on the basis of references [14, 17, 18], sliding mode control (SMC) of three-channel interleaved, two-stage paralleled buck DC-DC converter is analyzed in theory, simulated by means of MATLAB/SIMULINK and implemented in practice with current limitation, constant switching frequency and output voltage steady-state error, which outputs rated current of 260A and rated DC voltage of 150V. The paper is organized as below:

In section 2, introduction to PCM platform and its block diagram, topology of multi-channel interleaved, multi-stage paralleled buck DC-DC converter, the VA characteristics of plasma cutting power supply;

In section 3, state space model of buck DC-DC converter，introduction to SMC, SMC application to DC-DC Converters，selection of sliding line;

In section 4, practical issues of interleaved and paralleled buck converters, including current limitation, power equilibrium or current sharing, constant switching frequency, output current steady-state error.

In section 5, simulation by means of MATLAB/ SIMULINK, design and implementation of plasma cutting machine (PCM) DC current supply.

2 Specifications of PCM

2.1 Introduction to PCM platform

Plasma cutting machines includes two important parts: mechanical structure and electrical control, where the latter includes plasma cutting power supply, computer numerical control system (CNC) and arcing-box, control box, water cooling systems, and other necessary parts, such as valves and the torch. Typical plasma cutting machine system is shown in Fig.1 [1].
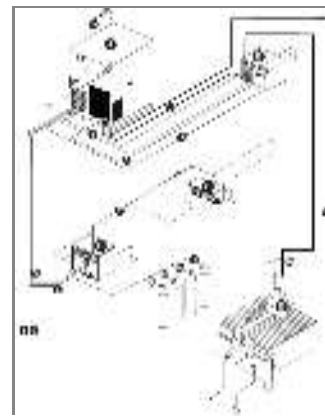

Fig.1 Block diagram of the PCM system

In Fig.1, system components include A－power supply; B－ignition console; C－off-vale assembly; D－gas console; E－torch. Cables and hoses include 1－Pilot arc lead; 2－Negative lead; 3－Ignition console power cable; 4－Ignition console coolant hoses; 5－Gas control cable; 6－Gas power cable; 7－Gas console to off-valve hose and lead assembly; 8－CNC interface cable; 9－Optional CNC interface cable for systems with multiple power supplies; 10－Torch lead assembly; 11－work lead; Supply gas hoses include 12－Oxygen; 13－Nitrogen or argon; 14－Air; 15－Argon-hydrogen (H35) or nitrogen-hydrogen (F5); Main power cable includes 16－Customer-supplied power cable.

Plasma cutting machine is an intelligent mechatronic equipment, integrated with power flow, information flow and control flow. Plasma cutting power source is one of the key components, mainly determining the quality of cutting current, such as stability, precision and speed of response, and then determine the workpiece cutting quality.

Principle of plasma cutting is: to make use of the high temperature of plasma arc column to make the metal workpiece molten and cut (evaporated),

and to get rid of molten metal to form cut via the plasma's momentum, suitable for cutting stainless steel, cast iron, copper, aluminum and other nonferrous metal tube and metal sheet, the thickness up to 35mm or more. Plasma arc beam itself has good mobility and diffusivity, good electrical conductivity and thermal conductivity, with its hundreds of times of the specific heat capacity at high temperature (proportional to the temperature). Actually, plasma cutting power supply is a kind of DC voltage to DC current converter.

At present, plasma current goes up to 1000A. Take plasma current of 260A for instance, the main electrical parameters are listed below:

AC input voltage (V): three-phase 380±15%; output DC current (A): 260; no-load output voltage (V): 310; working voltage (V): 150~170; step-down transformer (V/VV): 380/220/220, Y/YY connection, or to use more secondary windings, in order to support greater power output and improve the quality of the mains current; rated power factor: not less than 0.92; work duty rate (45.5kW,40°c): 100%, EMC regulation: EN61000-2-2/12.

2.2 VA characteristics of plasma power supply

Considering the static characteristic of plasma arc and the variation of arc length during cutting process, in order to keep the power supply stable, when arc voltage fluctuates, the current should be unchanged or changed slightly, the output of the plasma power source should have the sharp or vertical droop characteristic. For plasma cutting machine, except that PMSM based servo driver is responsible for horizontal movement of the torch, and DCM based servo driver is responsible for vertical movement of the torch, which maintains the length of arc within a reasonable range and keep the cutting current constant indirectly.

As for plasma power source, the external characteristic should be intersected with volt-ampere characteristic of plasma arc, shown in Fig.2. The condition of stable operation point can be expressed as below [14,17,18]:

$$\begin{cases} u_1 = u_2 \\ -\dfrac{du_1}{dt} \ge \dfrac{du_2}{dt} \end{cases} \tag{1}$$

where u_1 is the power supply voltage; u_2 is the arc voltage.

The drop rate of external characteristic of power supply should be faster than that of volt-ampere characteristics of the plasma arc, or else the arc will put out easily. In the vicinity of current setting, the output voltage has a quick and obvious change than that of output current, apparently showing as a DC current source. The current setting is determined by the material and thickness of the cut workpiece.
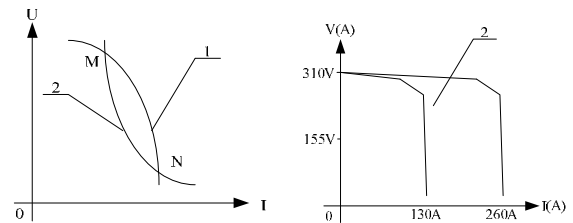

Fig.2 1－external characteristic of power supply;
2－volt-ampere characteristics of the plasma arc

2.3 Topology of buck DC-DC converter

Non-isolated buck DC-DC converter and isolated inverter-rectifier can be used as power supply of plasma cutting machine. To accommodate the requirements of cutting thicker work piece, high power output power supply is inevitable.

Three-channel interleaved two-stage paralleled buck DC-DC converter is employed as plasma cutting power supply, shown in Fig.3, which can support output DC current up to 750A and selected as the concerned topology in the paper.
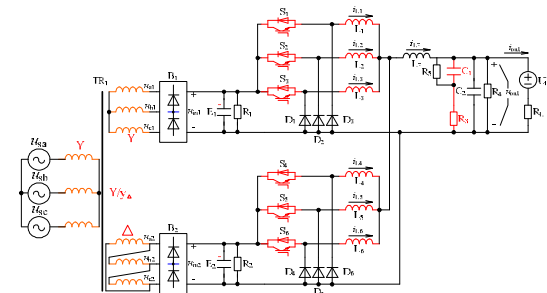

Fig.3 Three-channel interleaved two-stage paralleled buck DC-DC converter

Single-channel two-stage paralleled buck DC-DC converter can output DC current of 260A, which is the commonly used plasma cutting power supply at present, shown in Fig.4.
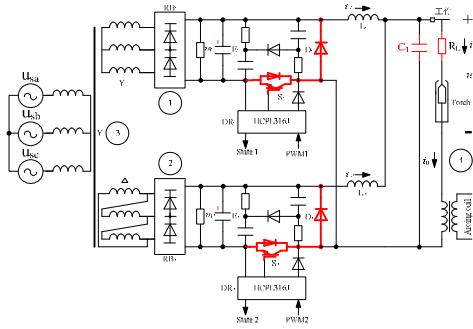

Fig.4 Single-channel two-stage paralleled buck DC-DC converter

As for Fig.3, define S_i is binary logic switching function for reverse conduction switch (RCS), where i=1, 2, 3, 4, 5 and 6. When the S_i is switched on, S_i=1, or else S_i=0.

According to reference [16], plasma power supply produces the arc column, like constant current supply. The approximate voltage across the plasma arc column can be expressed as

$$u_o = k_1 i_o + (20 + k_2 L_2) = k_1 i_o + E_o \qquad (2)$$

where u_o is the output voltage, that is, the voltage between cathode and workpiece; i_o is the output current or load current; L_2 is the distance between cathode and workpiece; k_1 is a small constant, relevant to load current; k_2 is a constant, relevant to plasma arc column.

In the steady state, neglecting the ripple, the average value of i_o is I_o. The amplitude of I_o depends on the different torch and workpiece.

Three-channel interleaved, two-stage paralleled buck DC-DC converter can be equivalent to six-stage paralleled buck DC-DC converter.

In Fig.3, for PCM, R_3 and C_1 constitute a series LC filter, R_4 and C_2 constitute a parallel LC filter, R_5 is a resistance with high value. The actual filter is more complicated. Each smoothing reactor has its own reversely-paralleled RCD as absorber.

When output current is 260A, the rated output voltage is 150V or so, and the equivalent resistance is roughly 0.58Ω. Practically, R_3=10Ω/50W,

R_4=100kΩ/25W, R_5=10k//10k//10k/25W, C_1=350μF/450V, C_2=0.22μF/120V, therefore R_4, R_5 and C_2 can be ignored, even more, R_3 branch can also be omitted. The control over the buck DC-DC converter is actually to control the current through L_7 and voltage across C_1, to control the currents through reactor L_1－L_6.

3 Principles of SMC

3.1 State Space Model of buck DC-DC converter

Assuming that distribution resistance of smoothing reactor is R_{Li}, the forward conduction voltage of power switch is near zero. The switching frequency is f_s, carrier frequency is f_c, then the current ripple frequency of L_7 is $6f_s$. L_7 is used to filter high frequency current ripple, designed with low inductance. For the convenience, L_7 can be omitted. For the six RCSs, given the duty cycle of the ith RCS in the kth switching period is d_{csi}, then

$$S_i = \begin{cases} 1, t_{ik} \leq t \leq t_{ik} + d_{csi} T_s \\ 0, t_{ik} + d_{csi} T_s \leq t \leq t_{i(k+1)} \end{cases} \qquad (3)$$

$$\left| t_{i(k+1)} = t_{ik} + T_s, k = 0,1,2,... \right.$$

where T_s is the switching period, t_{ik} is the initial time of the kth switching period for the ith RCS. Similarly, $t_{i(k+1)}$ can be dealt in the same manner.

Choose reactor currents (i_{L1}、i_{L2}、i_{L3}、i_{L4}、i_{L5}、i_{L6}) and output voltage (u_o) as the state variables.

Let $U_{in1} = U_{in2} = U_{in}$.

According to KVL,

$$L_i \frac{di_{Li}}{dt} = -L_7 \frac{di_{L7}}{dt} - R_{Li} i_{Li} - u_o + d_{csi} U_i \qquad (4)$$

$$6L_7 \frac{di_{L7}}{dt} = -\sum_{j=1}^{6} L_i \frac{di_{Li}}{dt} - \sum_{j=1}^{6} R_{Li} i_{Li} - 6u_o + \sum_{j=1}^{6} d_{csi} u_i \qquad (5)$$

According to KCL,

$$C_1 \frac{du_{c1}}{dt} = \sum_{i=1}^{6} i_{Li} - \frac{u_o}{R_L} + \frac{E_o}{R_L} = i_{L7} - \frac{u_o}{R_L} + \frac{E_o}{R_L} \qquad (6)$$

Due to $u_o = R_3 C_1 \frac{du_{c1}}{dt} + u_{c1}$, then

$$\frac{R_L + R_3}{R_L} C_1 \frac{du_{c1}}{dt} = i_{L7} - \frac{1}{R_L} u_{c1} + \frac{E_o}{R_L} \qquad (7)$$

The state space equations of the six-stage paralleled buck DC-DC converter are rewritten as below.

$$\begin{cases} \dfrac{di_{Li}}{dt} = -\dfrac{L_7}{L_i}\dfrac{di_{L7}}{dt} - \dfrac{R_{Li}}{L_i}i_{Li} - \dfrac{1}{L_i}u_{out} + \dfrac{1}{L_i}d_{csi}U_{in} \\[3mm] \dfrac{du_{c1}}{dt} = \dfrac{R_L}{C_1(R_L+R_3)}i_{L7} - \dfrac{1}{C_1(R_L+R_3)}u_{c1} \\[3mm] \qquad\quad + \dfrac{E_o}{C_1(R_L+R_3)} \end{cases} \quad (8)$$

3.2 Introduction to SMC[14, 17, 18]

The first substructure, referred as substructure I, is given by the following equations:

$$\begin{cases} \dot{x}_1 = x_2 \\ \dot{x}_2 = -K \cdot x_1 \end{cases} \quad (9)$$

where the eigenvalues are complex with zero real parts. The phase trajectories are circles, as shown in Fig. 5 and the system is stable marginally.

The second substructure, referred as substructure II, is given by

$$\begin{cases} \dot{x}_1 = x_2 \\ \dot{x}_2 = +K \cdot x_1 \end{cases} \quad (10)$$

In this case, the eigenvalues are real with opposite signs. The corresponding phase trajectories are shown in Fig.5, and the system is unstable. Only one phase trajectory, namely $x_2 = -qx_1 - \sqrt{K}x_1$ converges towards the origin, whereas all other trajectories are divergent.
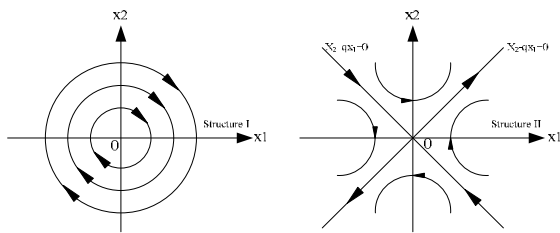

Fig.5 Phase-planes corresponding to substructures I and II

Partitioning the phase-plane in two regions, shown in Fig.6, as follows:

Region I: $x_1(x_2+cx_1)<0$ →Substructure I
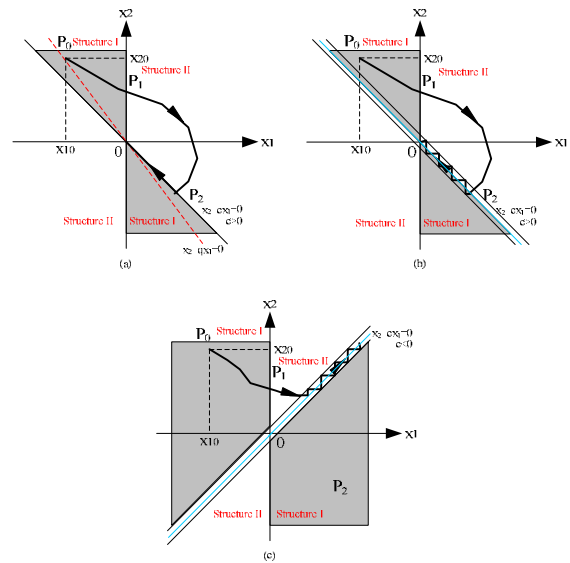Region II: $x_1(x_2+cx_1)>0$ →Substructure II

Fig. 6 Sliding regime. (a) ideal switching line; (b) switching line with hysteresis; (c) unstable sliding mode

In Fig.6, $c>0$ is lower than q. The switching boundaries are the x_2 axis and the line $x_2+cx_1=0$. The system structure changes whenever the system representative point (RP) enters a region defined by the switching boundaries. The important property of the phase trajectories of both substructures is that, in the vicinity of the switching line $x_2+cx_1=0$, phase trajectories will converge to the switching line. The immediate consequence of this property is that, once the RP hits the switching line, the control law ensures that the RP does not move away from the switching line.

Fig.6a shows a typical overall trajectory starting from an arbitrary initial condition $P_0(x_{10}, x_{20})$: after the intervals corresponding to trajectories P_0–P_1 (substructure I) and P_1–P_2 (substructure II), the final state evolution lies on the switching line (in the hypothesis of ideal infinite frequency commutations between the two substructures). This motion of the system RP along a trajectory is called the sliding mode, on which the structure of the system changes and which is not part of any of the substructure trajectories. The switching line $x_2+cx_1=0$ is called the sliding line. When sliding mode exists, the resultant system performance is entirely different from that dictated by any of the substructures of the VSS, and can be made independent of the properties of the substructures, dependent only on the control

law (in this case, the boundary $x_2+cx_1=0$). In this case, for example, the dynamic is of the first order with a time constant equal to 1/c. The independence of the closed-loop dynamics on the parameters of each substructure is not usually true for more complex systems, but in these cases it has been proved that the sliding-mode control shows better robustness than other control techniques. For higher-order systems, the control rule can be written in the following manner:

$$\sigma = f(x_1, x_2, ..., x_N) = \sum_{i=1}^{N} c_i x_i = 0 \qquad (11)$$

where N is the system order and x_i are the state variables. This will result in a particularly simple implementation in SMPS, if a linear combination of state variable in Eq.3 is employed. When the switching boundary isn't ideal, that is, the commutation frequency between the two substructures is limited, and the system RP trajectory is as shown in Fig.2b. Of course, the width of the hysteresis band beside the switching line determines the switching frequency between the two substructures.

Considering the following generalized system with scalar control [6, 7]:

$$\dot{x} = f(x,t,u) \qquad (12)$$

where x is a column vector; f is a function vector, with dimension of N, and u is an element which determines the system motion (control law). Considering that the function vector f is discontinuous on a surface $\sigma(x, t)=0$.

The above equation can be rewritten as follow.

$$\dot{x} = f(x,t,u) = \begin{cases} f^+(x,t,u^+) & \text{for } \sigma \to 0^+ \\ f^-(x,t,u^-) & \text{for } \sigma \to 0^- \end{cases} \qquad (13)$$

where the scalar discontinuous input u is given by

$$u = \begin{cases} u^+ & \text{for } \sigma(x) > 0 \\ u^- & \text{for } \sigma(x) < 0 \end{cases} \qquad (14)$$

The system is in sliding mode if its representative point moves on the sliding surface $\sigma(x, t)=0$.

3.3 SMC application to generic DC-DC Converters [14, 17, 18]

The general sliding mode control scheme of DC-DC converters is shown in Fig.7, where u_i and u_o are the input and output voltages, respectively, while i_{Li} and u_{Cj} (i=1, …, r, j=r+1, …, N-1) are the internal state variables of the converter (inductor currents and capacitor voltages). Switch S accounts for the system nonlinearity and indicates that the converter may assume only two linear sub-topologies, each associated to one switch status. All DC-DC converters having this property (including all single-switch topologies, plus push-pull, half and two-level full-bridge converters) are represented by the equivalent scheme of Fig.7. The above condition also implies that the sliding mode control is valid only for continuous conduction mode (CCM) operation.
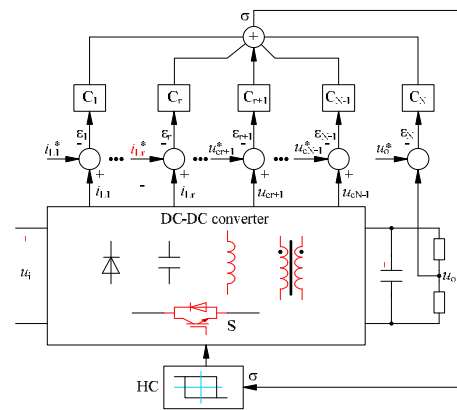

Fig.7 Principle scheme of a SM controller applied to DC-DC converters

As for the scheme in Fig.7, according to the general sliding mode control theory, all state variables are sensed, and the corresponding errors (defined by the difference to the steady-state values) are multiplied by proper gains c_i and added together to form the sliding function σ. Then, hysteretic block HC maintains this function near zero, so that

$$\sigma = \sum_{i=1}^{N} c_i \varepsilon_i \qquad (15)$$

Observe that Eq.15 represents a hyperplane in the state error space, passing through the origin. Each of the two regions separated by this plane is associated, by block HC, to one converter sub structure. If assuming (existence condition of the sliding mode) that the state trajectories near the

surface are directed towards the sliding plane, the system state can be enforced to remain near (fall into) the sliding plane by proper operation of the converter switches. Sliding mode controller design requires only proper selection of the sliding surface Eq.19, that is, coefficients c_i, to make sure existence, hitting and stability conditions. From a practical point of view, the selection of the sliding surface is not difficult if it is a second-order converters. In this case, the above conditions can be verified by simple graphical techniques. However, for higher-order converters, like Cúk and SEPIC converters, the more general approach must be rearranged. One of the major problems of the general scheme in Fig.7 is that inductor current and capacitor voltage references are difficult to evaluate, because they generally depend on load power demand, supply voltage and load voltage. It is true for all basic topologies, except the buck DC-DC converter, whose dynamic equations can be expressed in canonical form. Thus, for all converters, except the buck DC-DC topology, some provisions are needed to estimate the references, which will strongly affects the closed-loop dynamics.

3.4 SMC application to buck DC-DC Converters[14, 17, 18]

The most important features of the sliding mode regimes in VSS is the independence of responses to system parameter variation with the only constraint of canonical form description of the system. The buck DC-DC converter is particularly suitable for the sliding-mode control, just because the controllable states (output voltage and its derivative) are all continuous and accessible for measurement.

In order to guarantee the dynamic power equalization (current sharing) among the paralleled sub-converters, the jth reactor current can be represented by the following expression.

$$i_{Li} = \frac{1}{n-1} \sum_{\substack{j=1 \\ j \neq i}}^{6} (i_{Li}); j = 1, 2, 3, 4, 5, 6 \tag{16}$$

To satisfy the above conditions, the discontinuous control law d_{csi} of the ith sub-converter

must be switched with a sliding surface, and the sliding surface should include the information about the current of the ith paralleled sub-converter.

It is more convenient to use the system description, which involves the output error and its derivative, that is,

$$\begin{cases} x_1 = u_o - U_o^* \\ x_2 = \dfrac{dx_1}{dt} = \dfrac{U_o}{dt} = \dfrac{i_{C1}}{C_1} \end{cases} \tag{17}$$

Considering state variables x_1 and x_2, and a continuous conduction mode (CCM) operation, the system equations can be written as

$$\begin{cases} \dot{x}_1 = x_2 \\ \dot{x}_2 = -\dfrac{x_1}{LC} - \dfrac{x_2}{RC} + \dfrac{1}{LC}(U_i - U_o^*)u \end{cases} \tag{18}$$

where u is the discontinuous input, $u=1$ means reverse conduction switch is switched ON, and $u=0$ means switched OFF.

Rewrite the above equation in state space form.

$$\dot{x} = Ax + Bu + D \tag{19}$$

where

$$A = \begin{bmatrix} 0 & 1 \\ -\dfrac{1}{LC} & -\dfrac{1}{RC} \end{bmatrix}, \ B = \begin{bmatrix} 0 \\ \dfrac{U_i}{LC} \end{bmatrix}, \ D = \begin{bmatrix} 0 \\ -\dfrac{U_o^*}{LC} \end{bmatrix}$$

Practically, the damping factor of this second-order system is less than 1, resulting in complex conjugate eigenvalues with negative real part. The phase trajectories corresponding to the substructure $u=1$ are shown in Fig.8a for different values of the initial conditions. The equilibrium point for this substructure is $x_{1eq} = U_i - U_o^*$, $x_{2eq} = 0$. With $u=0$ the corresponding phase trajectories are reported in Fig.8b and the equilibrium point for this second substructure is $x_{1eq} = -U_o^*$, $x_{2eq} = 0$.

The boundary of this region can be derived from the constraint $i_L=0$ and is given by the equation:

$$x_2 = -\frac{1}{RC}x_1 - \frac{U_o^*}{RC} \tag{20}$$

which corresponds to the straight line with a

negative slope equal to $-1/RC$ and passing through the point $(-U_o^*, 0)$ shown in dashed line in Fig.8b. In the same figure, the line $x_1 = -U_o^*$ is also drawn, which defines another physically inaccessible region of the phase-plane, namely the region in which $u_o < 0$.
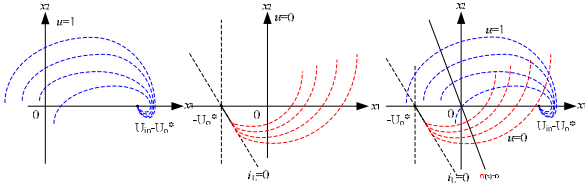

Fig.8 (a) Phase trajectories corresponding to u=1; (b)Phase trajectories corresponding to u=0; (c)Subsystem trajectories and sliding line

3.5 Selection of the Sliding Line[14, 17, 18]

It is convenient to select the sliding surface as a linear combination of the state variables, because the real control system is simple to design and equivalent control can be used to describe the system dynamic in sliding mode. Thus, sliding surface is given

$$\sigma(x) = c_1 x_1 + x_2 = C^T x = 0 \tag{21}$$

where $C^T = [c_1, 1]$ is the vector of sliding surface coefficients, and coefficient c_2 was set to 1 without loss of generality.

As shown in Fig.8c, this equation describes a line in the phase-plane, which passes through the origin, representing the stable operating point of the converter (zero output voltage error and its derivative).

$$\sigma(x_1, \dot{x}_1) = 0 \tag{22}$$

$$\sigma(x) = c_1 x_1 + \dot{x}_1 = 0 \tag{23}$$

which completely describes the system dynamic in sliding mode. If the existence and reaching conditions of the sliding mode are satisfied, a stable system will be obtained by choosing a positive c_1. Fig.8c reveals the great potentialities of the phase-plane representation for second-order systems. When choosing the following control law:

$$u = \begin{cases} 0 \ \text{for} \ \sigma(x) > 0 \\ 1 \ \text{for} \ \sigma(x) < 0 \end{cases} \tag{24}$$

the existence and reaching conditions are satisfied at the same time, at least in a small region around the system equilibrium point. By using this control law, on both sides of the sliding line, the phase trajectories of the corresponding substructures are directed toward the sliding line.

From Eq. (23), it is easy to see that the output voltage dynamics in sliding mode is simply given by a first-order system with time constant equal to $1/c_1$. Typical waveforms when $c_1 = 0.8/RC$ are shown in Fig. 9.
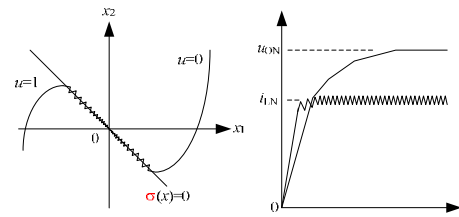

Fig.9 (a) Phase trajectories for two different initial conditions ($c_1 = 0.8/RC$); (b) Time responses of normalized output voltage u_{oN} and output current i_{LN} ($c_1 = 0.8/RC$) (initial RP in P1)

The increase of c_1 value causes a reduction of sliding-mode existence region. The sliding line coefficient c_1 also determines the system dynamic response in sliding mode, since the system dynamic response results are of first order with a time constant $\tau = 1/c_1$. Therefore, when $\tau < RC$, the resultant high response speed will narrow the existence region of the sliding mode. This can cause overshoots and ringing during transients.

4 Principles of SMC

4.1 Current Limitation[14, 17, 18]

According to reference [14, 17, 18], a fast output voltage dynamic causes overshoot of the inductor current i_L. The first part of the transient response depends on the system parameters, and only when the system representative point (RP) hits the sliding line at a point belonging to the existence region, the system dynamic is dictated by the sliding equation. For the buck DC-DC converter, it is actually dependent not the converter parameters but the sliding coefficient c_1.

The large inductor current brings about lots of shortcomings, including magnetic core saturation, over-current protection, and over high surging

voltage, etc. Current limitation can be easily incorporated into the sliding-mode controller by means of proper modification of the sliding line. For buck DC-DC converter, current limitation can be implemented by forcing the system RP on the new line:

$$x_2 = -\frac{1}{RC}x_1 + \frac{I_{Lmax}}{C} - \frac{U_o^*}{RC} \qquad (25)$$

Thus, the global sliding line consists of two pieces:

$$\sigma'(x) = \begin{cases} \dfrac{1}{RC}x_1 + x_2 - \dfrac{I_{Lmax}}{C} + \dfrac{U_o^*}{RC} \\ c_1x_1 + x_2 \end{cases} \qquad (26)$$

The phase plane trajectories for a buck DC-DC converter with inductor current limitation and with $c_1 = 2/RC$ are shown in Fig.10, and the corresponding normalized inductor current transient behavior is shown in Fig.10. It is interesting to note that Eq. (26) gives an explanation of why the fastest response without overshoots is obtained for $c_1 = 1/RC$. In fact, if $c_1 = 1/RC$ and $I_{Lmax} = U_o^*/R$, the two pieces of the sliding line σ' become a single line and thus the inductor current reaches its steady-state value U_o^*/R, without overshoot.
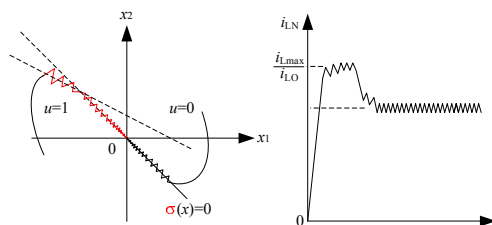

Fig.10 (a) Phase trajectories for a buck DC-DC converter with inductor current limitation ($c_1 = 2/RC$); (b) Time responses of normalized output current i_{LN} ($c_1 = 2/RC$)

4.2 Sliding-Mode Control Implementation[14, 17, 18]

Compared with the current control, some aspects of the sliding mode approach should be improved.

The first problem is that the switching frequency depends on the rate of change of function σ and on the amplitude of the hysteresis band.

Since σ is a linear combination of state variable errors, it depends on actually the produced currents and voltages, and its behavior may deviate from prediction. This system will be out of control, if the

range of variation becomes too high. One possible solution to the problem is to use a variable hysteresis band. For example, to use a PLL (phase locked loop). Another simple approach is to inject a suitable constant frequency signal w into the sliding function as shown in Fig.11[10].
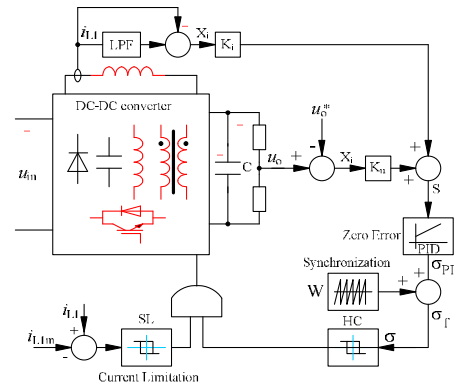

Fig. 11 Reduced-order sliding-mode controller with inductor current limitation, constant switching frequency, and without output voltage steady-state error

In the steady state, if the amplitude of w is predominant in σ_f, then a commutation occurs at any cycle of w. This also allows converter synchronized to an external trigger. Instead, under dynamic conditions, error terms x_i and x_u increase, w is overridden, and the system retains the excellent dynamic response of the sliding mode. Simulated waveforms of ramp w, and σ_{PI}, σ_f signals are reported in Fig.12.
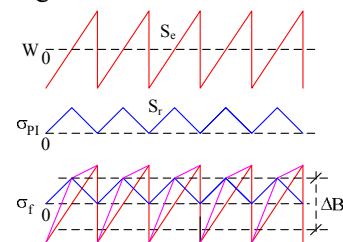

Fig. 12 Schematic waveforms of ramp w, and σPI, σf signals

But the amplitude of ramp signal w is worthy of further consideration. When selected, the slope of function σ_{PI} and the amplitude of hysteresis band should be determined so that function σ_f hits the lower part of the hysteresis band at the end of the ramp, as can cause the commutation.

From the analysis of the waveform shown in Fig.12, we can find that the slope S_e of the external ramp must satisfy the following inequality.

$$S_e > \frac{\Delta B}{\delta T_s} - S_r \qquad (27)$$

where ΔB represents the hysteresis band amplitude and S_r is the slope of function σ_{PI} during the switching-on time. Note that, in the presence of an external ramp, signal σ_{PI} must have a nonzero average value to accommodate the desired converter duty cycle (see Fig.12). Triangular disturbing signal w is not the only waveform that can be used. Pulse signal can also be employed alternatively [16].

The second problem rests with steady state error of the output voltage. When the inductor current reference comes from a low-pass filter, naturally the current error leads to zero average value in steady state. Therefore, if the sliding function has nonzero average value, due to the hysteretic control or due to the added ramp signal w, the steady-state output voltage error certainly appears. This problem can be solved by introducing a PI regulation on sliding function to eliminate its DC value (see Fig.11). In practice, the integral action of this regulator is enabled only when the system is on the sliding surface. In this way, the system behavior during large transients isn't affected, when σ can be far from zero, still maintaining the large-signal dynamic characteristics of sliding-mode control. A general-purpose sliding-mode controller scheme that includes the aforementioned improvements and a possible implementation of current limitation by means of another hysteretic comparator and an AND port, is shown in Fig.11.

4.3 SMC of paralleled n-buck DC-DC converters[14, 17, 18]

The new sliding mode surface is defined in function of $<u_o, i_c, i_{Lj}>$ and expressed by:

$$\dot{\sigma}_j(e_v, \dot{e}_v, e_{ij}) = \frac{1}{C_j} i_{Cj} + \alpha e_v + \beta e_{ij} \qquad (28)$$

The discontinuous control law is defined by:

$$v_j = \begin{cases} E_j; & \text{if } \sigma < 0 \\ 0; & \text{if } \sigma > 0 \end{cases} \qquad (29)$$

where v_j is the jth component of control; σ_j is the jth

component of the n sliding surfaces; e_{ij} is the jth current error defined by

$$e_{ij} = \frac{1}{n}\left\{ (n-1)i_{Lj} - \sum_{\substack{k=1 \\ k \neq j}}^{n} i_{Lk} \right\} \qquad (30)$$

where j=1,2,…, n; n is the number of the paralleled buck DC-DC converter; $\beta_j > 0$, a constant gain.

Fig.13 shows the block diagram of the SMC strategy, where $i_{ref} = \frac{1}{n}\sum_{k=1}^{n} i_{Lk}$.
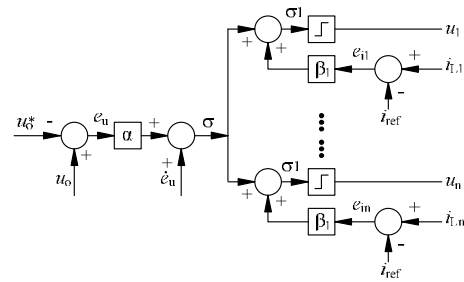

Fig.13 Block diagram of SMC over six paralleled buck DC-DC converter

The goal of VSS control through sliding mode scheme is to force the system to reach a prescribed ideal sliding surface. The existence condition for a sliding mode implies that the state trajectories on either side of the surface must be directed towards the sliding surface $s_j=0$ at least in an infinitesimal neighborhood. Mathematically the existence condition for sliding modes to occur on j^{th} surface may be stated by [14]:

$$\lim_{\sigma_j \to 0^+} \dot{\sigma}_j < 0 < \lim_{\sigma_j \to 0^-} \dot{\sigma}_j \qquad (31)$$

or by the equivalent inequality:

$$\lim_{\sigma_j \to 0} \sigma_j \dot{\sigma}_j < 0 \qquad (32)$$

The condition (33) is referred as the existence condition for sliding regime on the surface $\sigma_j=0$.

4.4 DESIGN of SMC[14, 17, 18]

The control design is obtained from the above equations and inequality (27). The procedure of design is summarized as follows:

Step 1: $\dot{\sigma}_j$ calculation for j = 1,2,...,n:

$$\dot{\sigma}_j = \frac{1}{C_j}\dot{i}_{Cj} + \alpha\,\dot{e}_v + \beta\,\dot{e}_{ij} \qquad (33)$$

#Step 2: existence condition calculation.

From equation (33), the conditions for sliding mode to occur on either side of $s_j = 0$ are:

If $\sigma_j < 0$, then $\upsilon_j = E_j$, j=1, 2, $\cdots$, n;

If $\sigma_j > 0$, then $\upsilon_j = 0$, j=1, 2, $\cdots$, n.

The ideal SMC operates at an infinite switching frequency that can't be implemented in practical systems. In order to reduce the switching frequency, several reduction methods, well- known in power electronics, can be employed. Among them the hysteresis control approach [14] is used.

The action controller is given by:

$$v_j = \begin{cases} E_j & \text{if } \sigma < -\Delta\sigma_j \\ 0 & \text{if } \sigma > \Delta\sigma_j \end{cases} \qquad (34)$$

where $\Delta\sigma_j$ establishes a symmetrical neighborhood to the switching surface and limits the maximum switching frequency.

5 Simulation and Implementation

5.1 Simulation of SMC based PCM power supply

According to power stage (in Fig. 3 and 4), and also after integrating SMC (in Fig.7, 11 and 13), two new SMCs are designed with the following features: current limitation (as rated current), power equilibrium or current sharing, constant switching frequency (10kHz), output current steady-state error, phase-shift driving and PID control.

At first the SMCs are simulated thoroughly by means of MATLAB/ SIMULINK according to the practical working conditions of PCM, which is shown in Fig.14, including power stage and control stage with ode23(mod. stiff/trapezoidal) for solver, discrete for simulation type, 1e-6s for sample time, and K_P=0.1, K_I=0.1 for the PI regulator.
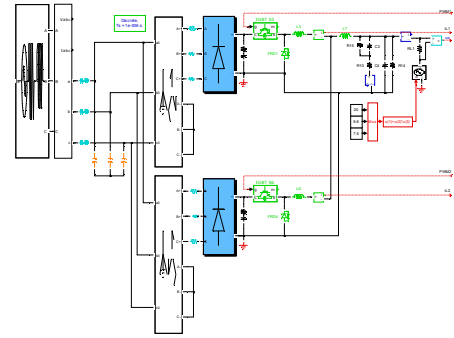
(a) Power stage
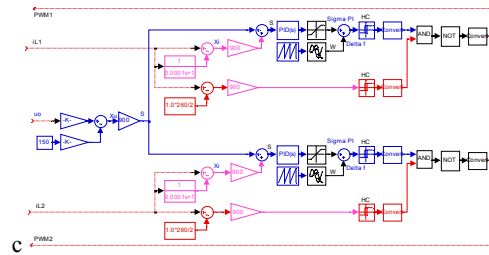
(b) Control stage 1 (Based on Fig.7 and 13)
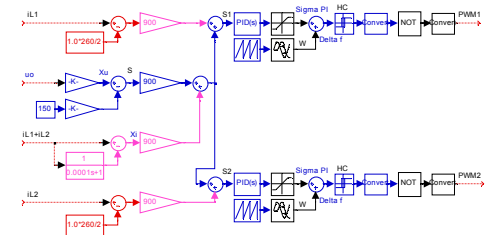
(c) Control stage 2 (Based on Fig.11 and 13)

Fig.14 Simulation circuit of SMC on two paralleled buck DC-DC converter

The main parameters are listed below:

There-phase input AC voltage is 380V/50Hz; there-phase output AC voltage of the step-down transformer with two separated winding is 220V/50Hz, Y/YΔ; For the buck DC-DC sub-converter, the rated output current is 130A, and the rated output voltage is 150V; the peak to peak current ripple is less than 5A; the switching frequency is 10kHz; the nominated inductance of reactor is 2.2mH/130A/35T, made of silicon steel. The selected inductances of reactors are 1.98mH and 2.42mH, respectively; the mains side LC filter is characteristic of inductance of 0.5mH/75A and capacitance of 2.2μF; the total electrolysis capacitor bank is of 4x6800μF/450V.

Considering plasma cutting is more complicated, and it is required to start the buck

DC-DC converter after power-up, thus the initial voltage value of electrolysis capacitor is set 310V.

Under the rated operation conditions, the waveforms of entire output voltage and output current are shown in Fig.15. Those of output current for the two sub-converters in Fig.16. As we can see that the maximum output current is limited, the power distribution is equal between two sub-converters due to the same average current, and output current is basically free of error in steady-state and without obvious overshoot in dynamic-state. In addition, the switching frequency is constant, and phase-shift driving and PID control are employed.

The resultant sliding trajectory of SMC is shown in Fig.17. The representative point reaches the origin from the initial condition (-150, 0) through near 7ms after the start of simulation.
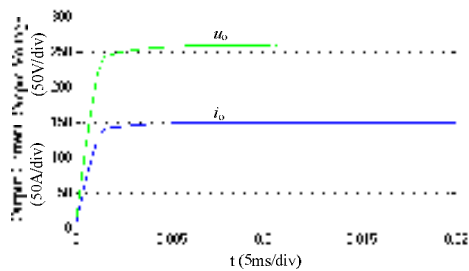

Fig.15 Simulated waveforms of entire output voltage and output current for buck DC-DC converter
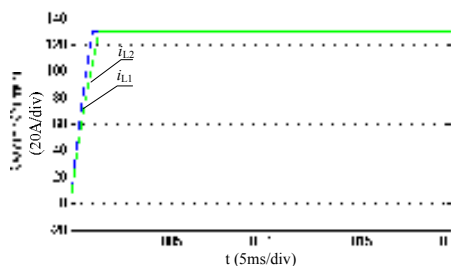

Fig.16 Simulated waveforms of output current for each buck DC-DC converter
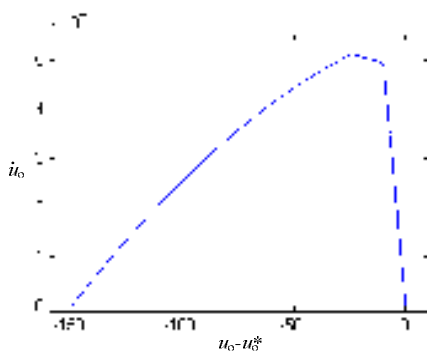

Fig.17 Simulated sliding trajectory of SMC

5.2 Implementation of SMC based PCM power supply

After theoretical analysis and simulation analysis, the fully-digital controlled plasma cutting power supply and complete PCM are developed successively, including computer numerical controller (CNC), torch height controller (THC), ignition console, gas console, water cooler, off-vale assembly, and so on. Several PCM sets are put into test on the market.

The design specifications are the same as those in simulation on the large, except that the real inductances of reactors are about 2.15mH and 2.30mH, respectively. The design of power circuit is in the form of power module, easy to assemble and disassemble. One leg module SKM300GB063D is selected as IGBT and FRD, F28335 is used as the kernel controller, which supports floating point operation. The switching part of buck DC-DC converter is shown in Fig.17.

Fig.17 Power circuit of two-stage paralleled buck DC-DC converter

After long time repeatedly regulation, the two paralleled buck DC-DC converter shows a satisfactory experimental results, and the work-piece cutting quality is high satisfactorily. When operating at the output current of 260A, the tested waveforms of output voltage and output current for are shown Fig.18, the total peak to peak current ripple is less than 5A, and the steady state error is not large than 1A.
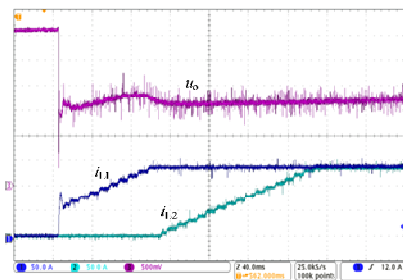
Fig.18 Tested waveforms of output voltage and output current for buck DC-DC converter

6. Conclusions

The DC current supply of plasma cutting machine is the typical application of high power buck DC-DC converter. In order to maintain and improve the whole power performance of the DC current supply, by using sliding mode control, the multi-channel interleaved multi-stage paralleled buck DC-DC converter is investigated in the paper, including theoretical analysis, simulation analysis and experimental verification. An single-channel interleaved two-stage paralleled buck DC-DC converter is designed and implemented with rated output voltage of 150V and rated output current of 260A, which is powered by three-phase AC power supply and step-down transformer. According to references [14, 17,18], two new sliding mode control (SMC) are made out and employed together, which features current limitation, power equilibrium, constant switching frequency, zero output current steady-state error and phase shift driving. Consequently, simulation and experimental results show that the proposed control strategy can make the designed DC current supply exhibit a good dynamic and static performance under severe load and disturbance conditions, and the high current precision, good stability and reliability bring about satisfactory cutting quality.

References

[1] HPR260XD Man Gas IM (806349). *Revised edition 1* [M] , Hypertherm, 2009.11.

[2] Ruixiang Hao, Qionglin Zheng, Xiaofie You, Wenjie Guo, Fei Lin, Characteristic analysis and experimental research on high-power plasma arc heater power supply, *Transaction of China Electrotechnical Society*, 2007, Vol. 22, Sup.1, pp. 78-82. (in Chinese)

[3] Jian Wu, Research on high-performance plasma cutting power supply system, *A thesis in Electrical Engineering for the Degree of Master of Engineering*, Nanjing University of Aeronautics and Astronautics. March, 2010. (in Chinese)

[4] Yaoling Chen, IGBT inverted plasma cutting power supply, *A thesis in Electrical Engineering for the Degree of Master of Engineering.* Lanzhou University of Science and technology, May, 2008. (in Chinese)

[5] Baoqi Liu, Shanxu Duan, Xun Li, An improved double closed loop control strategy for air plasma cutting converter, Przeglad Elektrotechniczny (Electrical Review), 2012, Vol. 88, No. 2, pp.278-282.

[6] V. I. Utkin, *Sliding modes and their application in variable structure systems*, MIR publishers, Moscow, 1978.

[7] U. Itkis, *Control Systems of Variable Structure*, John Wiley & Sons, New York, 1976.

[8] R. Venkataramanan, A. Sabanovic, S. Cúk, Sliding-mode control of DC-to-DC converters, *IECON Conf. Proc.*, 1985, pp. 251–258.

[9] K. Siri, C. Q. Lee, Current distribution control of converters connected in parallel, Proceedings of the *IEEE IAS*, Oct., 1990, pp.1274-1280.

[10] C. Q. Lee, K. Siri, T. F. Wu, Dynamic current distribution control of a parallel connection converter system, *IEEE PESC'91*, June 1991, Cambridge, MA, pp. 875-881.

[11] R. Wu, T. Kohama, Y. Kodera, T. Ninomiya, F. Ihara, Load-current-sharing control for parallel operation of DC-to-DC Converters, *IEEE PESC'93*, June 1993, pp. 101-107.

[12] P. F. Donoso-Garcia, P. C. Cortizo, B. R. Menezes, M, A. S. Mendes. Sliding mode control for current distribution in DC-DC converters connected in parallel, *IEEE-PESC'96*, 1996, Italy, pp. 1513-1518.

[13] I. Batarseh, k. Siri, H. Lee, Investigation of the output droop characteristic of parallel-connected DC-DC converter, *IEEE-PESC'94*, June 1994, Taiwan, China, pp.1342-1351.

[14] P.F. Donoso-Garcia, P.C. Cortizo, B.R. De Menezes, M.A. Severo Mendes, Sliding-mode control for current distribution in parallel-connected DC-DC converters, *IEE Proceedings Electric Power Applications*, Vol.145, No.4, Jul 1998, pp. 333-338.

[15] J. Fernando Silva, Sonia S. Paulo, Fixed frequency sliding mode modulator for current mode PWM inverters, *IEEE PESC'93*, 1993, pp. 623–629.

[16] Fo. B. J. Cardoso, B. R. Menezes, A. F. Moreira, P. C. Cortizo, Analysis of switching frequency reduction methods applied to sliding-mode controlled DC-DC

converters, *IEEE PESC'92*, June 1992, pp.403-410.

[17] Timothy L. Skvarenina, *The power electronics handbook. Purdue University*, Chapter 8: sliding-mode control of switched-mode power supply, West Lafayette, Indiana, 2002, CRC Press.

[18] Mousumi Biswal, Control techniques for dc-dc buck converter with improved performance, *A thesis submitted in partial fulfillment of the requirements for the degree of master of technology (research)*, Electrical Engineering, National Institute of Technology Rourkela, March 2011.

[19] -

[20] --------------------------